Case Studies in Thermal Engineering 50 (2023) 103410

Contents lists available at ScienceDirect

Case Studies in Thermal Engineering

journal homepage: www.elsevier.com/locate/csite

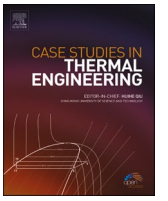

Numerical investigation of form-stable composite phase change material for battery passive cooling

Shi Chen, Ruiqi Wang *, Huashan Bao, Anthony Paul Roskilly, Zhiwei Ma

Department of Engineering, Durham University, Durham, DH1 3LE, UK

A R T I C L E I N F O

Handling Editor: Huihe Qiu

Keywords:
Form-stable composite PCM
Electric vehicle battery
Passive cooling
Numerical investigation

A B S T R A C T

Phase change material (PCM) has gathered much attention in battery thermal management for electric vehicles, in which form-stable PCM is a promising method to reduce the leakage of energy storage material. In this paper, a composite PCM that has form-stable property is used for passive cooling of electric car battery. Three cooling configurations are set up in the gap between two batteries, and their performance is analysed by a numerical model. The results show that integrating composite PCM with forced air convection can maximally prevent battery from heat accumulation at 5C and reduce the core temperature by 15.9 K, while filling the gap with composite PCM can reduce the temperature by 15.7 K. With the discharge rate decreased, forced air convection plays more significant role than PCM in slowing down the rise in battery temperature. The maximum battery temperature reduces when the ratio of PCM thickness to battery width increases from 0 to 0.1, but the maximum temperature is limited to a certain level with thicker PCM. The addition of 4.6 wt% graphite to the composite PCM greatly improved the heat absorption capacity of PCM, and the forced air with 20 $m \cdot s^{-1}$ velocity has better cooling behaviour than PCM.

Nomenclatures

Symbol	*Meaning*	*Units*
A	Surface area	m^2
c_p	Specific heat	$J \cdot kg^{-1} \cdot K^{-1}$
h	Heat transfer coefficient	$W \cdot m^{-2} \cdot K^{-1}$
H	Height	m
I	Current	A
l	Length	m
L	Latent heat	$J \cdot kg^{-1}$
n	Number of battery charge/discharge rate	
Nu	Nusselt number	\
p	Pressure	$N \cdot m^{-2}$
Pr	Prandtl number	\
q	Volumetric heat generation rate	$W \cdot m^{-3}$

* Corresponding author.
E-mail address: ruiqi.wang@durham.ac.uk (R. Wang).

https://doi.org/10.1016/j.csite.2023.103410
Received 10 December 2022; Received in revised form 9 August 2023; Accepted 21 August 2023
Available online 23 August 2023

Q	Heat flow quantity W
u	Flow velocity $m \cdot s^{-1}$
U	Open circuit potential V
V	Cell potential V
Vol	Volume m^3
R	Resistance Ω
Re	Reynolds number \
t	Time s
T	Temperature K
x	Distance from the leading edge m

Acronyms	*Symbol Meaning*
1-D	One-dimensional
BMS	Battery management system
BTMS	Battery thermal management system
EG	Expanded graphite
EV	Electric vehicle
HDPE	High density polyethylene
HEV	Hybrid electric vehicle
Li-ion	Lithium-ion
PA	Paraffin
PCM	Phase change material
SOC	State of charge

Greek symbols	*Symbol Meaning*	*Units*
ρ	Density	$kg \cdot m^{-3}$
λ	Thermal conductivity	$W \cdot m^{-1} \cdot K^{-1}$
ω	Mass fraction	\
μ	Fluid viscosity	$N \cdot s \cdot m^{-2}$
φ	Volume fraction of the disperse phase	\

Subscripts	*Symbol Meaning*
0	Reference environment
∞	Free stream conditions
amb	Ambient
b	Battery
c	Continuous phase
com	composite
conv	Convection
d	Disperse phase
dis	Discharge
e	Effective phase
E	East
f	Fluid
gen	Generation
l	Liquid
max	Maximum
P	Pole
s	Solid
W	West

1. Introduction

Development of electric vehicle (EV) and hybrid EV (HEV) is gathering momentum in recent years because of its eco-friendly features. As the depletion of fossil fuels and the global warming, EV/HEV continues to be entrusted with important role in the coming future. The performance of the EV/HEV strongly depends on the battery pack which undergoes thousands of charge and discharge cycles during the life of a vehicle [1]. Temperature increases when battery releasing the energy, and non-uniformity distribution of temperature are the major concern of the battery design and operation. In general, temperature impacts various aspects of battery performance, including its power capability, charging efficiency, lifespan etc. [2]. Considering that the EV/HEV normally operates over a range of weather conditions, effectiveness and reliability of battery are crucial [3].

Lithium-ion (Li-ion) battery is emerging as the most suitable technology for EV/HEV, mainly because of its higher energy density [4]. Safety issues surrounding Li-ion battery have been endlessly discussed, among which the most important element is its thermal performance [5]. A high battery operation temperature would accelerate thermal runaway and power fading of Li-ion cell if the accumulated heat is not removed properly and effectively [6,7]. Improving thermal performance of the battery can be achieved by reducing the heat generation rate of the battery and increasing the heat dissipation rate. Meanwhile, the battery thermal management system (BTMS) as part of battery management system (BMS) is essential to be used to maintain the operation temperature within the recommended operation temperature range. Battery thermal models have been developed coupling with the electrical model to predict the evolutions of the batter temperature and to ensure a good battery behaviour [8,9]. The traditional BTMS techniques based on air and liquid heat transfer mediums have been widely investigated [10]. Free air convection is not sufficiently fast for reducing battery temperature, and the general solution is to optimise the structure design of an air-cooled battery [11], or to create a forced convection cooling [12]. Forced air cooling system has the advantages such as simplicity of operation and electrical safety, whereas it still has a problem of lower heat transfer coefficient compared to liquid coolant system, causing it more difficult to unify the temperature on the pack [13]. Liquid-based cooling uses fluid coolant e.g., water, glycol, oil as mediums to cool the battery cell, but it usually comes with disadvantages like spare space, leakage, and complex design [14]. Under this situation, phase change material (PCM) passive cooling as a viable BTMS with simple design and low cost has drawn intensive research attention [1,15].

PCM has been popularly applied in thermal energy storage area. Commonly, PCM can absorb heat and change phase from solid to liquid, and it can release heat and change phase from liquid to solid in an opposite way. The energy absorbed by the PCM is mainly by means of latent heat which can store more quantities of energy than sensible heat. Advantages of PCM reflect in high potential for thermal energy storage and temperature control [16]. In the applications of EV/HEV, PCM can both reduce the maximum temperature and temperature unevenness in the battery pack [17]. A battery pack is composed of hundreds or thousands of cells modules. Configurations of PCM are normally set as wrapping around or locating between the cells of battery modules, so that heat generated from the cells can be input directly to the PCM [18,19]. Lots of experimental work were conducted to investigate the cooling efficiency of PCM and impact factors on the thermal management performance [20]. It was shown that cooling behaviour of PCM was affected by PCM structure, thickness, and phase change temperature. The combination of PCM with metal foam and fins was designed to wrap around a cylindrical battery pack for better cooling performance, and the work also revealed the melting characteristics of the PCM when heat is transferred from the battery to ambient [21]. In addition, selection of a PCM needs a few conditions which include high latent heat and suitable operation temperature of the battery pack [22]. Based on chemical constituents, PCM can be subdivided into three classifications, i.e., organic, inorganic, and eutectics PCMs [23]. Organic PCM presents superior characteristics to inorganic PCM due to its low corrosive properties and stable phase change temperature [1,24]. Among the extensive research of organic PCMs, paraffin (PA) wax that is mostly made up by a mixture of straight chain *n*-alkanes CH_3-(CH_2)-CH_3, has desired thermal performance, which has also been demonstrated its popularity as the PCM in the BTMS [25,26]. However, leakage of melted PA needs to be prevented by certain containers or tanks, resulting in more complex structure in practice.

Many strategies are developed to address the leakage problems, e.g., micro-encapsulated PCMs and form-stable PCMs [27,28]. Micro-encapsulated technique is used to produce PA into powder as the core-shell structure [29]. In contrast, form-stable PCM is shapable with more applications. To form the shape-stabilised PA, PA is usually blended with porous carbon materials or polymers, and it retains in solid state without volatilisation and leakage of liquid before and after the phase change [30]. Multiple materials such as polypropylene [31], expanded perlite [32], diatomite [33], high density polyethylene (HDPE) [34] etc., are used for PA as supported matrix. HDPE shows a little effect on the melting point of PA, which becomes a promising candidate for preparation of form-stable PA [25,34]. Another problem of PA is low thermal conductivity, since the average thermal conductivity of PA is only 0.2 $W{\cdot}m^{-1}{\cdot}K^{-1}$ [35]. Therefore, materials with high thermal conductivity are added into composite PCM to enhance the heat transfer. Expanded graphite (EG) is a commonly used additive with a layered structure and has good thermal conductivity [36], and has been shown to have a more temperature delay effect on PCM [37]. Experimental work presented that the thermal conductivity of PA/HDPE composite PCM with adding 4.3 wt% EG was improved to 1.36 $W{\cdot}m^{-1}{\cdot}K^{-1}$, more than four times of that without EG Ref. [38]. Based on a creative polymer PCM that was constructed by a cross-linked polymeric backbone with stearyl side chains, adding EG delivered a high thermal conductivity of 2.33 $W{\cdot}m^{-1}{\cdot}K^{-1}$ without PCM leakage during the long-term operation [39]. Combining PA with plastics and EG can potentially have great performance in avoiding liquid leakage and improving thermal conductivity. Lots of research have focused on the property investigation of form-stable composite PCM, but studies of using PA/HDPE with EG into BTMS on EV/HEV are limited.

In this paper, a composite PCM consisting of PA, HDPE, and EG, which has form-stable property, is used in the field of BTMS. Meanwhile, forced air convection is also implemented to assist in BTMS with composite PCM. To achieve a comprehensive analysis of battery cooling system, a numerical model is developed and validated. Different cooling scenarios of battery are compared to analyse and improve the thermal performance of battery. Sensitivity analyses are also explored to investigate the effects of PCM thickness, thermal conductivity, and air velocity on the battery heat dissipation effects. This study could provide some insights into the design of battery protection systems that utilise form-stable composite PCM and forced air convection.

2. System description

2.1. Battery cooling system

A commercial prismatic LiFePO4 battery composed of numerous cells with 90 mm in height, 27 mm in thickness, 70 mm in width was selected as battery sample for BTMS studies [18]. The cells were connected in series in battery module, and all the cells were chosen from a same batch which contains $LiFePO_4$ as the material for cathode and carbon-based material as the anode. A separator is attached between two electrodes and electrolyte (alkyl carbonate + $LiPF_6$) allows ions to transfer through it [40]. Main parameters of a

single battery cell used in the simulation have been collected in Table 1. The rated capacity of the used battery module is 12 Ah, which indicates that the battery module can charge/discharge 12 A electricity for 1 h. Normally, this battery charge/discharge rate is named as 1C. If the same 12 A battery is charge/discharge at a 2C rate, 24 A electricity will be used/obtained or provided for 30 min. For battery charge/discharge at *n*C rate, the battery will work with 12n A current for $\frac{1}{n}$ hour. In this study, the battery is assumed to be charged/discharged at a constant current procedure of 1C, 3C, and 5C, respectively.

Battery internal resistance R_{dis} can be calculated based on the function of state of charge (SOC). Experimental results of R_{dis} have been fitted into Equation (1) [18]:

$$R_{dis}(SOC) = 0.00705 - 0.01853 \times SOC + 0.05894 \times SOC^2 - 0.09151 \times SOC^3$$

$$+0.06579 \times SOC^4 - 0.01707 \times SOC^5 \quad (1)$$

Four different scenarios of battery cooling are considered as shown in Fig. 1 in which the case 1 is a reference system that batteries are packed without any cooling methods. In case 2, composite PCM (PA mixed with HDPE and EG) is located between the battery cells on the largest surface side (YZ) of battery modules to assist in BTMS. Initial ratio between battery cell width and PCM thickness is set as 0.2. In case 3, battery is cooled by traditional forced air convection without placing PCM between cells. Cooling air would enter the space between cells at the YZ plane to transfer the excess heat. The gap that lets cooling air pass through between cells has the same width as the PCM thickness in case 2. In case 4, configuration that combines PCM with forced air cooling is brought forward to cool the batteries. Half of the PCM in case 2 is divided equally and placed on both side of cells, leaving middle gap for air convection.

2.2. Form-stable composite PCM

A commercial PA RT35HC supplied by Rubitherm® was used as PCM due to its proper melting point and high thermal energy storage capacity. The melting point needs to ensure that PCM returns easily from liquid to solid state at room temperature. The main properties of PCM are provided by the company as shown in Table 2.

HDPE was chosen as the supporting matrix which has good compatibility with PA. EG was used as a thermal conductivity enhancer of composite PCM. Values of properties of HDPE and EG are given in Table 3. To avoid seepage and keep the shape of PCM, the maximum weight percentage for PA dispersed in the composite PCM has been found through the experimental work as high as 77 wt% [43]. The percentage of HDPE in composite PCM should not be less than 23 wt% otherwise the leakage will happen. And when the percentage of EG is added to 3 wt%, thermal conductivity of composite PCM can be increased by 24%. Therefore, the ideal percentage of three materials to prepare the composite PCM to achieve form-stable property is recommended as 74.7 wt% paraffin, 22.3 wt% HDPE and 3 wt% EG. Such combination helps the composite PCM to keep a stable form during the phase change while improving the thermal conductivity. The bulk density of composite PCM is measured by weighting the material and measuring the volume.

When the composite PCM has no phase change happened, the specific heat capacity of composite PCM can be calculated based on the mass fraction of each material and their heat capacities, which could be expressed as Equation (2):

$$c_{p,com} = \omega_{HDPE} c_{p,HDPE} + \omega_{PCM} c_{p,PCM} + \omega_{EG} c_{p,EG} \quad (2)$$

where ω is the mass fraction of each component.

For the region of phase change, effective specific heat capacity of PCM is calculated by using the effective heat capacity method as shown in Fig. 2. The latent heat of PCM is depicted as a triangle shape surrounded by the effective specific heat capacity and the abscissa within a pre-defined temperature range from T_s to T_l. The used equations to calculate $c_{p,PCM}$ by triangle model are confirmed by Ma et al. as shown in Equations (3) and (4) [44]:

$$c_{p,PCM} = (T - T_s)\left[\frac{c_{p,PCM,l} - c_{p,PCM,s}}{T_l - T_s} + \frac{4\Delta L_{PCM}}{(T_l - T_s)^2}\right] + c_{p,PCM,s} \quad T_s \le T \le (T_s + T_l)/2 \quad (3)$$

$$c_{p,PCM} = (T_l - T)\left[\frac{4\Delta L_{PCM}}{(T_l - T_s)^2} - \frac{c_{p,PCM,l} - c_{p,PCM,s}}{T_l - T_s}\right] + c_{p,PCM,l} \quad (T_s + T_l)/2 \le T \le T_l \quad (4)$$

where L_{PCM} is latent heat of PCM, $c_{p,PCM,l}$ and $c_{p,PCM,s}$ are specific heat capacities of composite PCM with liquid and solid states, T_s and T_l

Table 1
Parameters of a battery cell.

Parameter	Value[a]
Specific heat capacity of cell, $c_{p,\ b}$	950 J·kg^{-1}·K^{-1}
Thermal conductivity of cell, $\lambda_{\ cell}$	2.6 W·m^{-1}·K^{-1}
Density of cell, ρ_{cell}	2335 kg·m^{-3}
Nominal voltage	3.2 V
Rated capacity	12 Ah
Weight of one battery cell	0.4 kg
Temperature coefficient of voltage, dU/dT	0.00022 V·K^{-1}

[a] The values were collected from the reference [18,41].

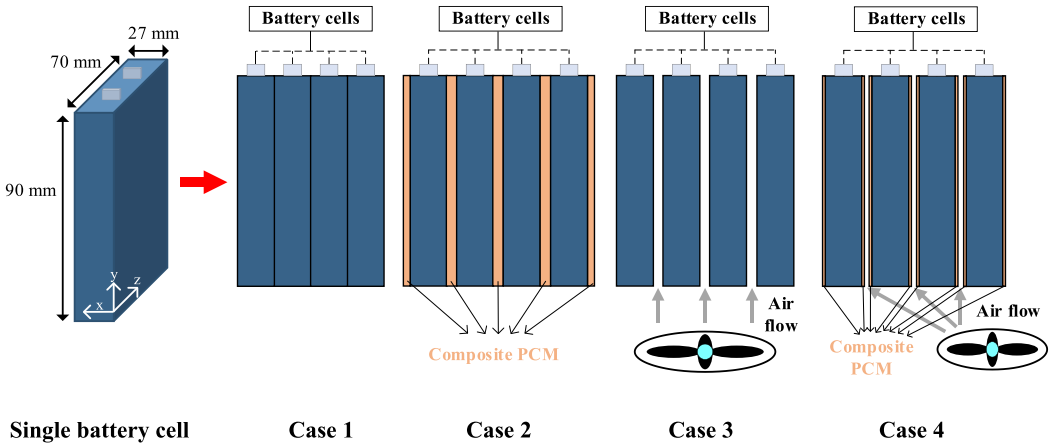

Fig. 1. Four cooling configurations of BTMS.

Table 2
Main parameters of PCM (RT35HC) [42].

Parameters	Value
Melting temperature	307.15 K–311.15 K
Heat storage capacity	240000 J·kg^{-1}
Specific heat capacity, $c_{p,\ PCM}$	2000 J·kg^{-1}·K^{-1}
Density solid, $\rho_{PCM,\ s}$	0.88 kg·L^{-1}
Density liquid, $\rho_{PCM,\ l}$	0.77 kg·L^{-1}
Heat conductivity (both phase), $\lambda_{\ PCM}$	0.2 W m^{-1}·K^{-1}
Volume expansion	12%
Flash point	450.15 K

Table 3
Main properties of HDPE and EG.

Parameters	HDPE	EG
Thermal conductivity, λ_{HDPE}, λ_{EG}	0.45–0.52 W·m^{-1}·K^{-1}	3 W·m^{-1}·K^{-1} [34]
Density, ρ_{HDPE}, ρ_{EG}	0.93–0.97 kg·L^{-1}	0.0035 kg·L^{-1} [34]
Specific heat capacity, $c_{p,\ HDPE}$, $c_{p,\ EG}$	1900 J kg^{-1}·K^{-1}	610 J·kg^{-1}·K^{-1}

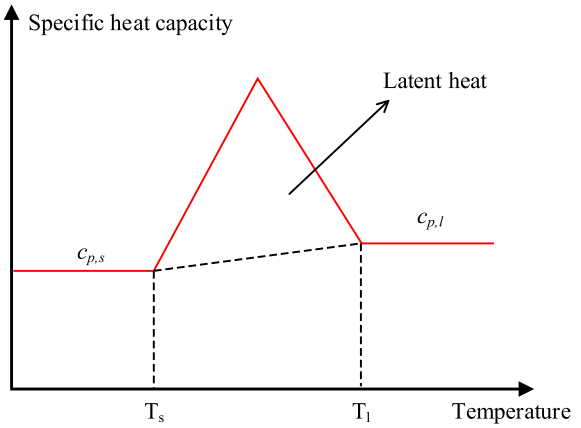

Fig. 2. Model of effective specific capacity of composite PCM [44].

are solid and liquid temperatures of PCM, respectively. Here, the T_s is set to the melting temperature of PCM as 308.15 K, and T_l is set to increase by 4 K to reach 312.15 K to ensure complete melting of the PCM.

For estimating the thermal conductivity of the composite PCM, the classic Maxwell-Eucken model is used, as given by Equation (5):

$$\lambda_e = \lambda_c \left[\frac{\lambda_d + 2\lambda_c + 2\varphi(\lambda_d - \lambda_c)}{\lambda_d + 2\lambda_c - \varphi(\lambda_d - \lambda_c)} \right] \tag{5}$$

where the subscripts e, c and d indicate effective, continuous phase and disperse phase respectively, φ is the volume fraction of the disperse phase. Here for the present composite PCM, HDPE is considered as continuous phase, PA-EG is considered as disperse phase (thermal conductivity of PA-EG is calculated first with EG as continuous).

The obtained properties of the developed PCM are shown in Table 4. Considering the narrow temperature range in the study, the temperature independent properties are used.

2.3. Air convective heat transfer coefficient

When a fluid with velocity u and T_f flows over a surface of area A, the total heat transfer rate $\dot{Q}_{conv}$ is obtained by integrating the heat fluid over the entire surface and is expressed as Equation (6) [45]:

$$\dot{Q}_{conv} = (T_s - T_f) \int_A h_{air} dA \tag{6}$$

where h_{air} is the convective heat transfer coefficient, A is the surface area of the subject where the pair passes through, T_s is the temperature of solid surface.

For the condition of forced air convection, the actual heat transfer coefficient depends upon multiple properties, including air flow velocity, and roughness of the solid surface. As shown in Fig. 3, it is assumed that the velocity of the air is zero at the surface of the object. When the air flow is generated by a fan to cool the battery, fluid will flow between two cells, which means that the air goes through the middle has the fastest velocity. Thus, velocity of the air could be calculated as an average value between the highest velocity and zero. In case 3 and 4, cooling air passes through YZ plane of cell and the plane can be assumed as a flat plate. In determining whether a fluid flow passing through the boundary layer is laminar or turbulent, it is frequently to calculate Reynolds number as Equation (7) [45]:

$$Re = \frac{\rho u_\infty x}{\mu} \tag{7}$$

where u_∞ is the relative velocity between object surface and air, μ is the viscosity of the fluid, x is the distance from the leading edge. A representative value of critical Re that decides the beginning of turbulence is 5×10^5. When 300 K air flows at 20 m·s^{-1} velocity over YZ plane of cell with 0.09 m length, critical location for transition from laminar to turbulent flow is calculated as 0.4 m, which is much longer than the length of cell. Therefore, calculation of air heat transfer coefficient in this study is based on the laminar equations.

To provide a measure of the convection heat transfer over a plate, Nusselt number is used to describe the temperature gradient at the surface as Equation (8) [45]:

$$Nu = \frac{hl}{\lambda_f} \tag{8}$$

where l is the length of flat plate. The averaged $\overline{Nu}$ for laminar flow over the entire surface is also a universal function of Re and Prandtl number (Pr), which can be calculated as Equation (9) [46]:

$$\overline{Nu} = \frac{\overline{h}l}{\lambda_f} = 0.664 Re_l^{1/2} Pr^{1/3} \quad Pr \geq 0.6, Re \leq 2 \times 10^5 \tag{9}$$

Referring thermal properties of air at 300 K and atmospheric pressure, ρ, μ, and λ for air are 1.1614 kg·m^{-3}, 1.846×10^{-5} N·s·m^{-2}, and 2.63×10^{-2} W·m^{-1}·K^{-1}, respectively [45]. Integrating Equations (7)–(9) and parameters, average heat transfer coefficient of air is simplified as:

$$\overline{h_{air}} = \frac{0.664 Re_l^{1/2} Pr^{1/3} \lambda_f}{l} = \frac{0.664 \rho^{1/2} u_\infty{}^{1/2} Pr^{1/3} \lambda_f}{(\mu l)^{1/2}} = 13 u_\infty^{1/2} \tag{10}$$

where Pr equals 0.707 when air flows over the cell surface at a temperature of 300 K. In this study, the cells module is tested in the fan

Table 4
Main properties of form-stable composite PCM (74.7 wt% PA + 22.3 wt% HDPE + 3 wt% EG).

Parameters	Bulk density	Specific heat	Thermal conductivity
Value	1000 kg m^{-3}	Solid: 1614 J·kg^{-1}·K^{-1} Liquid: 1936 J·kg^{-1}·K^{-1}	0.26 W·m^{-1}·K^{-1}

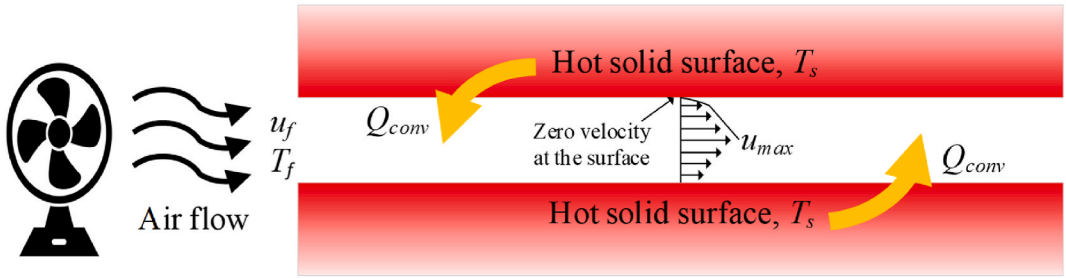

Fig. 3. Air forced convection, adapted from Ref. [46].

under air flow velocities of 1–20 m·s^{-1}. Various heat transfer coefficients will be calculated based on Equation (10) and be further used for evaluating impacts of air flow velocities on battery cooling performance. For the cases 1 and 2 that batteries are protected without using forced air convection, it is assumed that natural air convection happens at the batteries surface with air heat transfer coefficient of 2.25 W·m^{-2}·K^{-1} [18].

3. Modelling

3.1. Governing equations

A thermodynamic model is developed for thermal analysis of battery and PCM. MATLAB is used for the simulation of the battery cooling system. Due to the assumption of no leakage occurs during the phase change process of form-stable composite PCM, the heat conduction process is only considered across the battery and PCM as a one-dimensional (1-D) model (X direction), as shown in Fig. 4. Battery and PCM have the same height. The 1-D continuity equation for present model is given as [37]:

$$\frac{\partial \rho}{\partial t}+\frac{\partial(\rho u)}{\partial x}=0 \tag{11}$$

The 1-D steady state momentum equation is derived from Newton's second law of motion and is described as [45]:

$$u\frac{\partial u}{\partial x}=-\frac{1}{\rho}\frac{\partial p}{\partial t}+\mu\frac{\partial^2 u}{\partial x^2} \tag{12}$$

where p is the pressure and body forces are ignored here.

A 1-D heat conduction equation is used to describe this heat transfer process as following [45]:

$$\rho c_p\frac{\partial T}{\partial t}=\frac{\partial}{\partial x}\left(\lambda\frac{\partial T}{\partial x}\right)+\dot{q}_b \tag{13}$$

where $\dot{q}_b$ is the heat generated by the battery per volume (W·m^{-3}) and is only applied to battery. Because of using effective specific heat

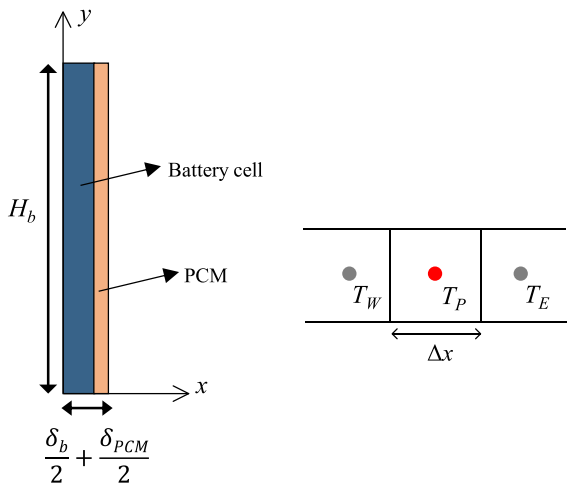

Fig. 4. Physical model of the passive PCM battery cooling system.

capacity, latent heat of PCM is not considered in above equation. The initial condition of heat conduction is expressed as Equation (14):

$$T|_{t=0} = T_{amb} \tag{14}$$

where T_{amb} is ambient temperature. Considering symmetry of two adjacent cells, following boundary condition (Equation (15)) is considered for a single battery cell (all four cases) and composite PCM (case 2).

$$\left.\frac{\partial T}{\partial x}\right|_{x=0, x=\frac{\delta_b}{2}+\frac{\delta_{PCM}}{2}} = 0 \tag{15}$$

And the contact surface of battery and PCM shares same boundary condition as Equation (16):

$$-\lambda_b \frac{\partial T}{\partial x} = -\lambda_{PCM} \frac{\partial T}{\partial x} \tag{16}$$

The air cooling boundary condition (case 3 and case 4) is formulated as Equation (17):

$$-\lambda \left.\frac{\partial T}{\partial y}\right|_{x=\frac{\delta_b}{2}, x=\frac{\delta_b}{2}+\frac{\delta_{PCM}}{2}} = h_{air}(T - T_{amb}) \tag{17}$$

where h_{air} is the forced convection heat transfer coefficient of air calculated by Equation (10).

Finite volume method is applied to transfer the above differential equation into algebraic form, which is then solved by implicit method, as shown in Equation (18):

$$\Delta x \rho c_p \frac{T_P - T_{P,0}}{\Delta t} = \lambda_{EP} \frac{T_E - T_P}{\Delta x} + \lambda_{WP} \frac{T_W - T_P}{\Delta x} + \Delta x \dot{q} \tag{18}$$

where λ_{EP} and λ_{WP} represent thermal conductivities in the directions of east to pole and west to pole, respectively. The output temperatures at the nodes of $x = 0, \frac{\delta b}{2}, \frac{\delta b}{2} + \frac{\delta PCM}{2}$ will be obtained from the model.

3.2. Heat generation by battery

To simply the simulation, the heat generation of Li-ion battery cells is spatially uniform. The simplified calculation of heat generation of battery that excludes the enthalpy of mixing and phase change terms can be shown as Equation (19) [40]:

$$\dot{Q}_{b,gen} = I(U - V) + IT \frac{dU}{dt} \tag{19}$$

where I is the current, U and V are the open circuit voltage and cell voltage, respectively. The equation is formulated based on the thermal characteristic and not considered the complex reaction in the cell. The term $IT\frac{dU}{dt}$ can be either exothermic or endothermic, thus the equation can be transferred as [18]:

$$\dot{Q}_{b,gen} = I^2 R_{dis} + IT \frac{dU}{dt} \tag{20}$$

Volumetric heat generation rate of the battery pack can be calculated as Equation (21), and

$$\dot{q}_b = \frac{I^2 R + IT \frac{dU}{dt}}{Vol_b} \tag{21}$$

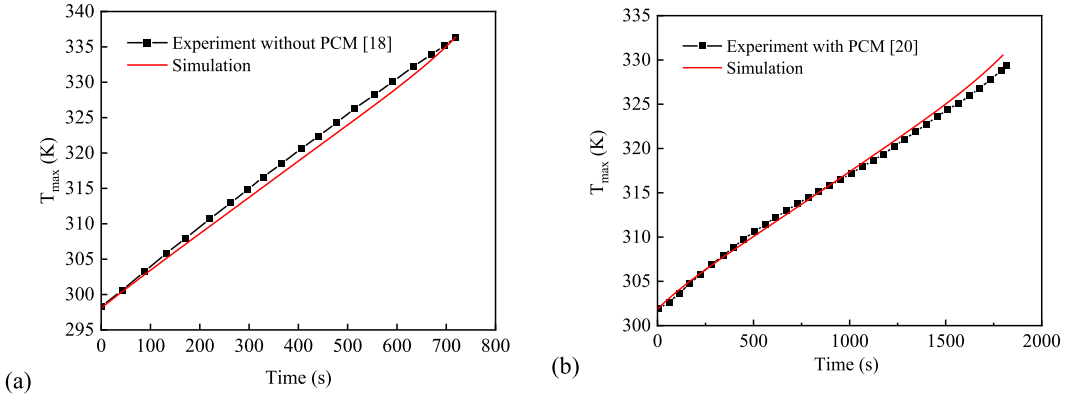

Fig. 5. The validation of battery heat generation model with experimental data: (a) without PCM; (b) with PCM.

where Vol_b is the battery volume. As shown in Table 1, $\frac{dU}{dt}$ is 0.00022 V·K^{-1}.

3.3. Model validation

The battery heat generation model has been validated by the experiments of the batteries with and without using PCM. The T_{max} of battery without PCM protection is compared with experimental data from the work [18]. Battery parameters used for simulation are listed in Table 1. Ambient temperature is set as 298.15 K. Battery cell constantly discharges at the rate of 5C. Similarly, the T_{max} of battery from model using PCM is compared with experimental results of the reference [20] which employed the battery with a capacity

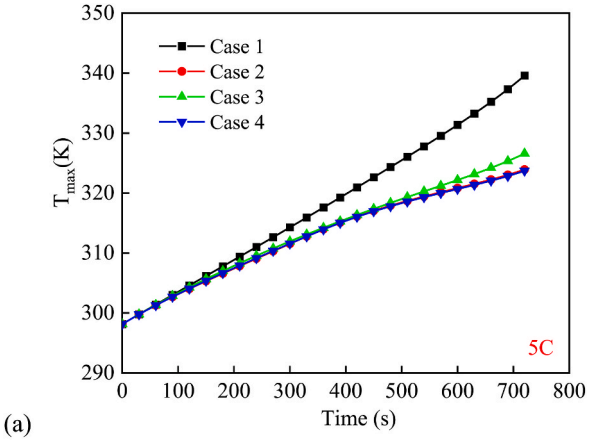

(a)

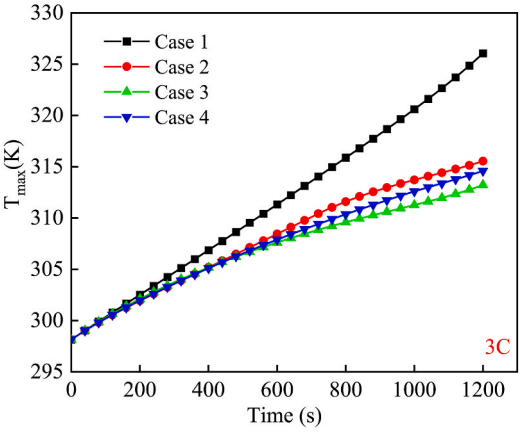

(b)

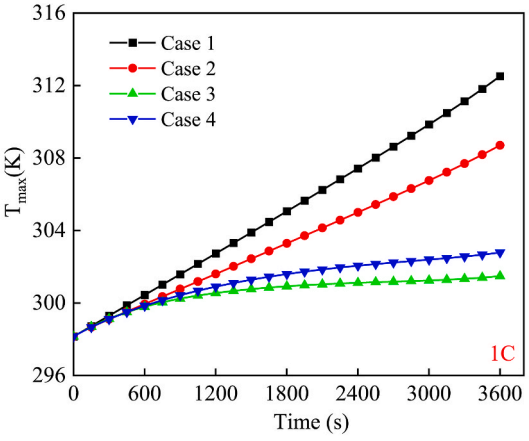

(c)

Fig. 6. Maximum temperature in the battery for different cases: (a) 5C, (b) 3C, (c) 1C.

of 27 Ah and discharging at 2C. The PCM in the experiment has 333.15 K phase change temperature and 25 mm thickness. Validated results of two simulation models are shown in Fig. 5. The curves show generally consistent changes among the simulated results and experimental values over the discharge time. Minor deviations between simulation and experiment probably attribute to 1-D model used in the simulation that ignores heat transfer from other directions. It is demonstrated that the battery heat generation model can well predict thermal performance of the cell, which is feasible to be used for the subsequent investigation of battery with different BTMSs.

4. Results and discussion

4.1. Comparison of different cooling scenarios

The influence of four BTMS configurations on the battery cooling is investigated in this section. In Fig. 6, tendencies of the maximum temperature which is also the cell core temperature are compared under four cooling conditions at the discharge rates of 5C, 3C, and 1C. For cases 3 and 4, heat transfer coefficient of forced air convection is 41.1 $W{\cdot}m^{-2}{\cdot}K^{-1}$ with a velocity of 10 $m{\cdot}s^{-1}$. It is significant that faster discharge rate leads to larger increased temperature of battery. When battery is discharged without any cooling method, i.e., in case 1, the temperature peaks of battery appear at the end of discharge stages, which are 339.6 K, 326.1 K, 312.5 K for 5C, 3C, 1C, respectively.

For the discharge rate of 5C, the T_{max} corresponding to cases 2, 3, 4 are 323.9 K, 326.5 K, 323.7 K, and the temperature differences are 15.7 K, 13.1 K, 15.9 K in compassion with T_{max} when no BTMS is deployed (case 1). It indicates that coupled PCM and forced air convection has the optimal cooling effect for battery, followed by independent utilisation of each method, and the variation trends of T_{max} for cases 2 and 4 are nearly consistent, meaning that PCM passive cooling can achieve the same function as forced air cooling at faster discharge rate. For 3C discharge, the temperatures at the end of discharging stage are 315.5 K, 313.2 K, 314.6 K for cases 2, 3, and 4, respectively. Therefore, the largest T_{max} difference occurs between case 1 and 3 with 12.8 K. Three BTMSs show the different cooling performance comparing with battery discharging at 5C. It is found that cooling of battery by forced air (case 3) considerably slows down the increase of battery temperature, resulting in the lowest final temperature of battery. Similar performance of forced air cooling also reflects at the lower discharge rate of 1C. The temperature in the case 3 has less rise than the temperature increments in the case 2 and case 4, which is 11.0 K lower than the T_{max} in the case of no BTMS. Although the heat removed by PCM in case 2 is obviously lower than cases 3 and 4, the battery temperature has been controlled within the range of phase change temperature of PCM, thus satisfying the cooling requirement. Significant rise of the T_{max} in the case 2 as shown in Fig. 6 (c) demonstrates that the melting of PCM is still proceeding.

4.2. Effects of PCM thickness

Evolutions of the battery maximum temperature under different cooling systems have demonstrated that PCM has impressive cooling performance for battery. PCM thickness is further to be discussed to investigate its effectiveness on the BTMS. Fig. 7 indicates the variations of battery temperature under the conditions of different PCM thickness in case 2. The value of x-axis represents the ratio of PCM thickness to battery width (thickness ratio). The sharp decrease in temperature when thickness ratio increases from 0 to 0.1 reflects the effectiveness of PCM cooling on battery. As shown in the figure, higher thickness ratio, i.e., thicker PCM has not visibly improved battery temperature due to the fixed melting temperature of PCM used in the simulation. Thus, ranges of temperature in which the battery could be cooled down (comparing to case 1) by PCM are limited around 16 K, 11 K, and 7 K for discharge rates of 5C, 3C, and 1C, respectively.

Detailed variations of temperature in case 2 with the increment of 0.02 for the thickness ratios in the range of 0–0.1 are shown in Fig. 8. Fig. 8 (a) shows the change profile of the T_{max} in the battery. When the thickness ratio is lower than 0.06, the T_{max} curves present

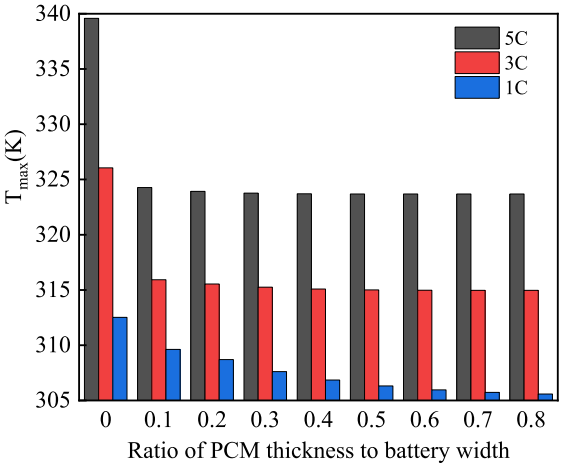

Fig. 7. Effects of PCM thicknesses on the maximum temperature in the battery (case 2).

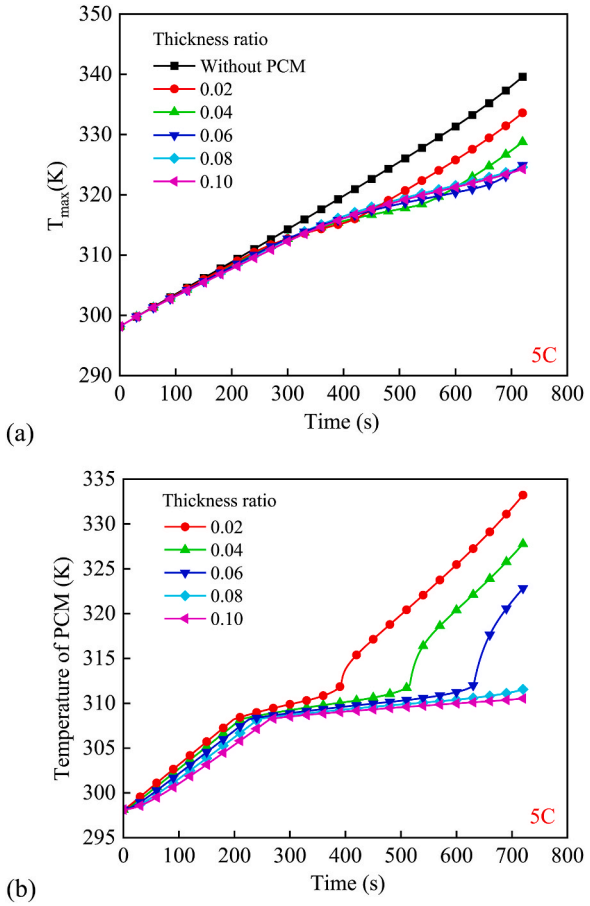

Fig. 8. Different thicknesses ratio of PCM/cell vs. (a) the maximum temperature in the battery; (b) the temperature of PCM.

swift increases after a period of steady temperature. This phenomenon proves that PCM has been completely melted by heat generated from battery. Due to thinner PCM, less heat can be absorbed and stored by PCM so that the battery temperature keeps increasing. Comparably, the T_{max} gradually rises to a plateau when the thickness ratio varies from 0.08 to 0.1. This is mainly because the PCM with thickness ratio higher than 0.08 has enough capacity to absorb and store the heat from battery. This effect can also be confirmed by variations of PCM temperature during the discharge process, as given in Fig. 8 (b). Apparent twists of PCM temperature happen at 388 s, 510 s, and 630 s which are related with thickness ratio of 0.02, 0.04, and 0.06, respectively, indicating the finish of melting of PCM. With the increase of thickness ratio, sufficient PCMs are possible to contain battery heat, thus their temperatures are maintained at melting points. As a result, the battery cooling effect of PCM varies significantly with the choice of PCM thickness, excessively thin PCM is not applicable for the BTMS, and thick PCM will suffer from the issues with high cost and size of thermal management system.

4.3. Effects of EG mass fraction

Besides thickness of PCM, thermal conductivity of composite PCM is another critical parameter needs to be discussed for its effects on battery cooling. The composite PCM in this study is investigated to be added into EG as thermal conductivity enhanced additives. Referring a group of measured thermal conductivities from Ref. [38] with the increase of EG weight as shown in Table 5, thermal conductivity of shape-stabilised PCMs increased from 0.31 $W{\cdot}m^{-1}{\cdot}K^{-1}$ to 1.36 $W{\cdot}m^{-1}{\cdot}K^{-1}$ when EG weight fraction was up to 4.6 wt%. These values are subsequently input into the model to compare the T_{max} of battery. Thickness ratio of PCM to cell is chosen as 0.2. Two scenarios that the PCM is assembled without (case 2) and with forced air cooling (case 4) are considered here, and the results are shown in Fig. 9.

In Fig. 9 (a), the increments of temperature fit into one line at initial phase until battery discharges at around 300 s. After this point,

Table 5
Thermal conductivity of PCM with increased EG mass fraction [38].

EG mass fraction (wt.%)	0	1	2	3	4	4.6
Thermal conductivity ($W{\cdot}m^{-1}{\cdot}K^{-1}$)	0.31	0.58	0.76	1.03	1.25	1.36

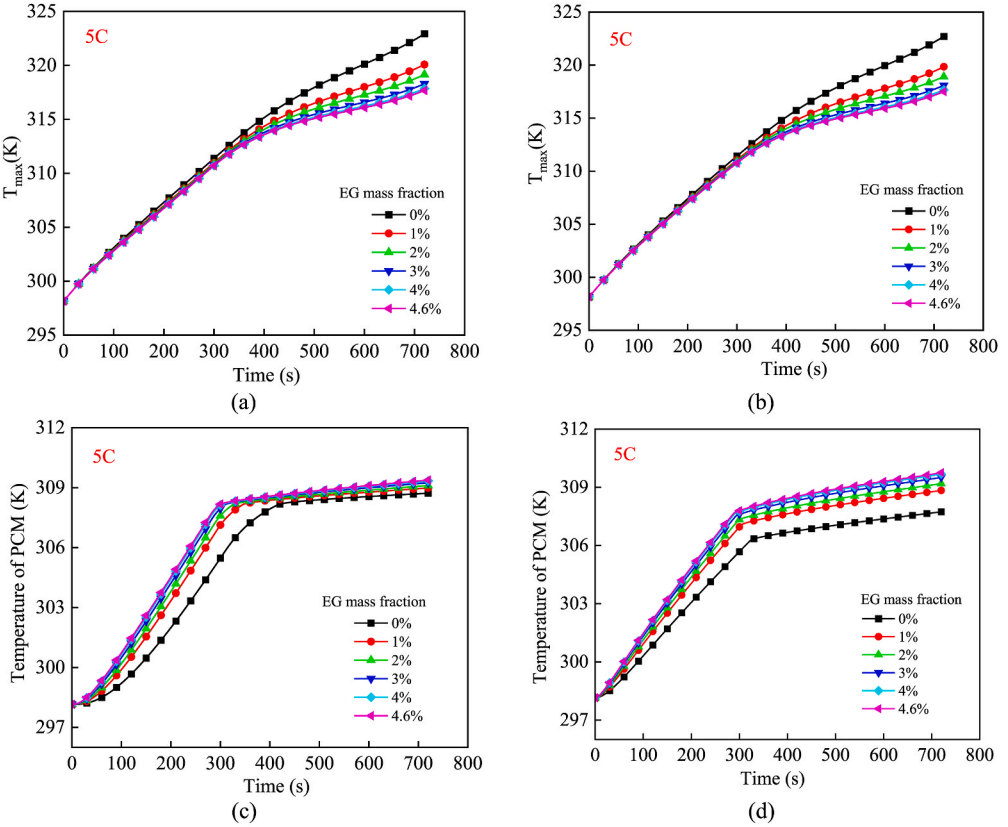

Fig. 9. Different PCM thermal conductivities vs. (a) the T_{max} of the battery (case 2); (b) the T_{max} of the battery (case 4); (c) temperature of PCM (case 2); (d) temperature of PCM (case 4).

the changes of the T_{max} appear divergence under different EG mass fraction. With higher quantity of EG in the composite PCM, better performance on controlling battery temperature can be found, which reveals that more EG in the PCM could promote thermal conductivity and therefore the heat transfer and cooling performance. The T_{max} at the end of discharge stage is 317.7 K when EG fraction is 4.6 wt%, much less than 322.9 K without any EG additives. In Fig. 9 (b), half PCM between the cells has been removed and the gap is used for air flow at 10 m·s^{-1} with 41.1 W·m^{-2}·K^{-1} heat transfer coefficient, and the results show the consistent variations of the T_{max} compared to case without forced air convection. Temperature gradients of case 4 are slightly lower than those of case 2, resulting the T_{max} of 317.5 K at the end of discharging. In order to shed light on combined effects of PCM and forced convection between two scenarios, Fig. 9 (c) and Fig. 9 (d) presents temperature lifts of the PCM in the discharge process of case 2 and case 4, respectively, when introducing different proportion of EG. It is observed that lower EG mass fraction decelerates upward trend of PCM temperature. In Fig. 9 (c), more EG inside PCM leads to larger amount of heat absorbed by the PCM, resulting heat accumulation in the PCM and temperature rising faster. When the temperature rises to a certain point, it starts the phase of smooth increasing until all the PCM finishing the melting. Similar PCM temperature profiles are also found in Fig. 9 (d), and the differences are subtle between two cases. With the help of forced air cooling, terminal temperature of PCM reaches up to 309.8 K at the highest EG mass fraction, which is 0.4 K higher than that in the case without air cooling. This finding demonstrates that the effect of thermal conductivity of PCM on BTMS is not singularly linear relationship, also depending upon the PCM thickness and the availability of air cooling.

4.4. Effects of cooling air flow velocity

To investigate cooling effects by forced air convection (case 3), the T_{max} of batteries are compared under the conditions of different air velocities. In Fig. 10, air flow velocity varies from 1 m·s^{-1} to 20 m·s^{-1} corresponding heat transfer coefficient of air from 13.0 W·m^{-2}·K^{-1} to 58 W·m^{-2}·K^{-1} according to Equation (10). When the battery is cooled only under forced convection condition without PCM, faster air velocity decreases the rising rate of the T_{max}. At the end of discharge, the T_{max} reaches 334.4 K under convection velocity of 1 m·s^{-1}, which can decline by 11.1 K using 20 m·s^{-1} air velocity. In comparison with battery temperature of case 2, only 20 m·s^{-1} air flow can achieve better performance than PCM on battery cooling. Enhancing air velocity would not have obvious effect on improving heat transfer coefficient when air passes through small gap between cells. Higher air velocity could also damage the structure and performance of battery. Therefore, at high and medium discharge rates, form-stable composite PCM is more suitable for BTMS.

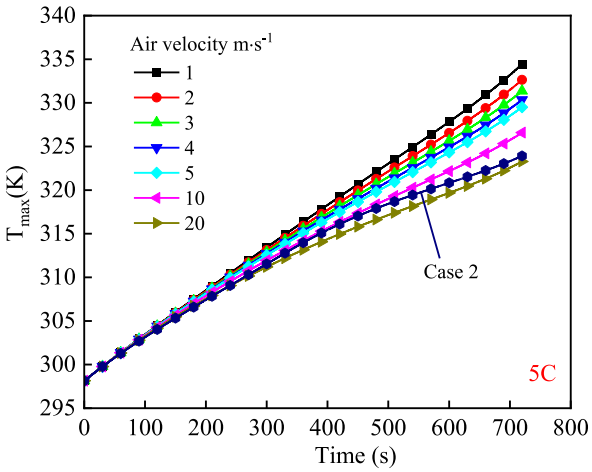

Fig. 10. Temperature of cell boundary with the change of forced air flow velocity.

5. Conclusions

A composite PCM consisting of PA, EG and HDPE, which has form-stable property, was used in this study to evaluate its effects on the battery cooling. A numerical model was developed to comprehensively analyse and compare different battery cooling configurations. Ideas for designing BTMS that considers form-stable composite PCM and forced air convection are summarised: (1) coupled composite PCM and forced air convection has the optimal cooling effect for battery cooling at 5C, resulting 15.9 K reduction in the maximum temperature (comparing to case 1), followed by 15.7 K reduction with the help of composite PCM only; (2) when considering slower discharge rate of battery, forced air convection is more effective in avoiding heat accumulation inside the battery; (3) the sensitivity analysis of PCM thickness revealed that the maximum battery temperature can reduce when the ratio of PCM thickness to battery width increases from 0 to 0.1, but the maximum temperature is limited to a certain level when the thickness of PCM constantly increases; (4) when mass fraction of EG in the composite PCM increases from 0 wt% to 4.6 wt%, the maximum temperature of battery is reduced from 322.9 K to 317.7 K at 5C, due to the improvement by EG on the thermal conductivity; (5) a possible velocity range of forced air showed that the maximum battery temperature can decline by 11.1 K using 20 $m \cdot s^{-1}$ air velocity. Based on different composite PCM and forced air cooling configurations between two batteries, suitable BTMS choices for the EV/HEV should depend on the actual discharge rate, PCM thickness, EG mass fraction, and air velocity, thereby reducing dissipation of PCM and complex structure.

CRediT author statement

Shi Chen: Conceptualization, Methodology, Writing - Original draft, Reviewing. Ruiqi Wang: Data curation, Software, Writing - Original draft, Reviewing and Editing. Huashan Bao: Supervision, Conceptualization, Methodology. Anthony Paul Roskilly: Supervision, Funding acquisition, Resources. Zhiwei Ma: Supervision, Software, Methodology, Writing - Reviewing and Editing.

Declaration of competing interest

The authors declare that they have no known competing financial interests or personal relationships that could have appeared to influence the work reported in this paper.

Data availability

Data will be made available on request.

Acknowledgement

This research was supported by Engineering and Physical Sciences Research Council (EPSRC) under Grant EP/V027050/1 (Industrial Decarbonisation Research and Innovation Centre - IDRIC) in the United Kingdom.

References

[1] M. Malik, I. Dincer, M.A. Rosen, Review on use of phase change materials in battery thermal management for electric and hybrid electric vehicles, Int. J. Energy Res. 40 (2016) 1011–1031, https://doi.org/10.1002/er.3496.
[2] A.A. Pesaran, Battery thermal models for hybrid vehicle simulations, J. Power Sources 110 (2002) 377–382, https://doi.org/10.1016/S0378-7753(02)00200-8.
[3] G. Zhao, X. Wang, M. Negnevitsky, H. Zhang, A review of air-cooling battery thermal management systems for electric and hybrid electric vehicles, J. Power Sources 501 (2021), 230001, https://doi.org/10.1016/j.jpowsour.2021.230001.

[4] F. Larsson, P. Andersson, B.-E. Mellander, Lithium-ion battery aspects on fires in electrified vehicles on the basis of experimental abuse tests, Batteries 2 (2016) 9, https://doi.org/10.3390/batteries2020009.
[5] D.H. Doughty, E.P. Roth, A general discussion of Li ion battery safety, Electrochem. Soc. Interface 21 (2012) 37–44, https://doi.org/10.1149/2.f03122if.
[6] P. Ramadass, B. Haran, R. White, B.N. Popov, Capacity fade of Sony 18650 cells cycled at elevated temperatures: Part II. Capacity fade analysis, J. Power Sources 112 (2002) 614–620, https://doi.org/10.1016/S0378-7753(02)00473-1.
[7] S.A. Khateeb, M.M. Farid, J.R. Selman, S. Al-Hallaj, Design and simulation of a lithium-ion battery with a phase change material thermal management system for an electric scooter, J. Power Sources 128 (2004) 292–307, https://doi.org/10.1016/j.jpowsour.2003.09.070.
[8] W. Li, Y. Xie, X. Hu, M.K. Tran, M. Fowler, S. Panchal, et al., An internal heating strategy for lithium-ion batteries without lithium plating based on self-adaptive alternating current pulse, IEEE Trans. Veh. Technol. 72 (2023) 5809–5823, https://doi.org/10.1109/TVT.2022.3229187.
[9] R. Braga, A. Mevawalla, S. Gudiyella, S. Panchal, M. Giuliano, G. Nicol, et al., Transient electrochemical modeling and performance investigation under different driving conditions for 144Ah Li-ion cell with two jelly rolls, SAE Technical Paper. 2023-01-0513, https://doi.org/10.4271/2023-01-0513, 2023.
[10] H. Park, A design of air flow configuration for cooling lithium ion battery in hybrid electric vehicles, J. Power Sources 239 (2013) 30–36, https://doi.org/10.1016/j.jpowsour.2013.03.102.
[11] Y. Xie, Y. Liu, M. Fowler, M.-K. Tran, S. Panchal, W. Li, et al., Enhanced optimization algorithm for the structural design of an air-cooled battery pack considering battery lifespan and consistency, Int. J. Energy Res. 46 (2022) 24021–24044, https://doi.org/10.1002/er.8700.
[12] Y. Wang, D. Dan, Y. Zhang, Y. Qian, S. Panchal, M. Fowler, et al., A novel heat dissipation structure based on flat heat pipe for battery thermal management system, Int. J. Energy Res. 46 (2022) 15961–15980, https://doi.org/10.1002/er.8294.
[13] S. Panchal, I. Dincer, M. Agelin-Chaab, R. Fraser, M. Fowler, Thermal modeling and validation of temperature distributions in a prismatic lithium-ion battery at different discharge rates and varying boundary conditions, Appl. Therm. Eng. 96 (2016) 190–199, https://doi.org/10.1016/j.applthermaleng.2015.11.019.
[14] Z. Rao, S. Wang, A review of power battery thermal energy management, Renew. Sustain. Energy Rev. 15 (2011) 4554–4571, https://doi.org/10.1016/j.rser.2011.07.096.
[15] L. Ianniciello, P.H. Biwolé, P. Achard, Electric vehicles batteries thermal management systems employing phase change materials, J. Power Sources 378 (2018) 383–403, https://doi.org/10.1016/j.jpowsour.2017.12.071.
[16] Y. Azizi, S.M. Sadrameli, Thermal management of a LiFePO4 battery pack at high temperature environment using a composite of phase change materials and aluminum wire mesh plates, Energy Convers. Manag. 128 (2016) 294–302, https://doi.org/10.1016/j.enconman.2016.09.081.
[17] J. Yan, K. Li, H. Chen, Q. Wang, J. Sun, Experimental study on the application of phase change material in the dynamic cycling of battery pack system, Energy Convers. Manag. 128 (2016) 12–19, https://doi.org/10.1016/j.enconman.2016.09.058.
[18] W. Wu, W. Wu, S. Wang, Thermal management optimization of a prismatic battery with shape-stabilized phase change material, Int. J. Heat Mass Tran. 121 (2018) 967–977, https://doi.org/10.1016/j.ijheatmasstransfer.2018.01.062.
[19] X. Duan, G.F. Naterer, Heat transfer in phase change materials for thermal management of electric vehicle battery modules, Int. J. Heat Mass Tran. 53 (2010) 5176–5182, https://doi.org/10.1016/j.ijheatmasstransfer.2010.07.044.
[20] Z. Zhou, D. Wang, Y. Peng, M. Li, B. Wang, B. Cao, et al., Experimental study on the thermal management performance of phase change material module for the large format prismatic lithium-ion battery, Energy 238 (2022), 122081, https://doi.org/10.1016/j.energy.2021.122081.
[21] H. Najafi Khaboshan, F. Jaliliantabar, A. Adam Abdullah, S. Panchal, Improving the cooling performance of cylindrical lithium-ion battery using three passive methods in a battery thermal management system, Appl. Therm. Eng. 227 (2023), 120320, https://doi.org/10.1016/j.applthermaleng.2023.120320.
[22] Z. Ling, Z. Zhang, G. Shi, X. Fang, L. Wang, X. Gao, et al., Review on thermal management systems using phase change materials for electronic components, Li-ion batteries and photovoltaic modules, Renew. Sustain. Energy Rev. 31 (2014) 427–438, https://doi.org/10.1016/j.rser.2013.12.017.
[23] F. Agyenim, N. Hewitt, P. Eames, M. Smyth, A review of materials, heat transfer and phase change problem formulation for latent heat thermal energy storage systems (LHTESS), Renew. Sustain. Energy Rev. 14 (2010) 615–628, https://doi.org/10.1016/j.rser.2009.10.015.
[24] J. Pereira da Cunha, P. Eames, Thermal energy storage for low and medium temperature applications using phase change materials – a review, Appl. Energy 177 (2016) 227–238, https://doi.org/10.1016/j.apenergy.2016.05.097.
[25] W. Wu, W. Wu, S. Wang, Form-stable and thermally induced flexible composite phase change material for thermal energy storage and thermal management applications, Appl. Energy 236 (2019) 10–21, https://doi.org/10.1016/j.apenergy.2018.11.071.
[26] R. Youssef, M.S. Hosen, J. He, M. Al-Saadi, J. Van Mierlo, M. Berecibar, Novel design optimization for passive cooling PCM assisted battery thermal management system in electric vehicles, Case Stud. Therm. Eng. 32 (2022), 101896, https://doi.org/10.1016/j.csite.2022.101896.
[27] M. Delgado, A. Lázaro, J. Mazo, B. Zalba, Review on phase change material emulsions and microencapsulated phase change material slurries: materials, heat transfer studies and applications, Renew. Sustain. Energy Rev. 16 (2012) 253–273, https://doi.org/10.1016/j.rser.2011.07.152.
[28] C. Chen, X. Liu, W. Liu, M. Ma, A comparative study of myristic acid/bentonite and myristic acid/Eudragit L100 form stable phase change materials for thermal energy storage, Sol. Energy Mater. Sol. Cell. 127 (2014) 14–20, https://doi.org/10.1016/j.solmat.2014.03.057.
[29] T. Khadiran, M.Z. Hussein, Z. Zainal, R. Rusli, Encapsulation techniques for organic phase change materials as thermal energy storage medium: a review, Sol. Energy Mater. Sol. Cell. 143 (2015) 78–98, https://doi.org/10.1016/j.solmat.2015.06.039.
[30] K. Wei, Z. Liu, L. Wang, B. Ma, Y. Fan, J. Shi, et al., Preparation of polyurethane solid-solid low temperature PCMs granular asphalt mixes and study of phase change temperature control behavior, Sol. Energy 231 (2022) 149–157, https://doi.org/10.1016/j.solener.2021.11.056.
[31] C. Alkan, K. Kaya, A. Sarı, Preparation, thermal properties and thermal reliability of form-stable paraffin/polypropylene composite for thermal energy storage, J. Polym. Environ. 17 (2009) 254, https://doi.org/10.1007/s10924-009-0146-7.
[32] A. Karaipekli, A. Biçer, A. Sarı, V.V. Tyagi, Thermal characteristics of expanded perlite/paraffin composite phase change material with enhanced thermal conductivity using carbon nanotubes, Energy Convers. Manag. 134 (2017) 373–381, https://doi.org/10.1016/j.enconman.2016.12.053.
[33] P. Zhang, Y. Cui, K. Zhang, S. Wu, D. Chen, Y. Gao, Enhanced thermal storage capacity of paraffin/diatomite composite using oleophobic modification, J. Clean. Prod. 279 (2021), 123211, https://doi.org/10.1016/j.jclepro.2020.123211.
[34] Y. Qu, S. Wang, Y. Tian, D. Zhou, Comprehensive evaluation of Paraffin-HDPE shape stabilized PCM with hybrid carbon nano-additives, Appl. Therm. Eng. 163 (2019), 114404, https://doi.org/10.1016/j.applthermaleng.2019.114404.
[35] P. Sobolciak, M. Karkri, M.A. Al-Maadeed, I. Krupa, Thermal characterization of phase change materials based on linear low-density polyethylene, paraffin wax and expanded graphite, Renew. Energy 88 (2016) 372–382, https://doi.org/10.1016/j.renene.2015.11.056.
[36] R. Taherian, Application of polymer-based composites: bipolar plate of PEM fuel cells, Electrical Conductivity in Polymer-Based Composites 7 (2019) 183–237, https://doi.org/10.1016/B978-0-12-812541-0.00007-0.
[37] V. Talele, M.S. Patil, S. Panchal, R. Fraser, M. Fowler, S.R. Gunti, Novel metallic separator coupled composite phase change material passive thermal design for large format prismatic battery pack, J. Energy Storage 58 (2023), 106336, https://doi.org/10.1016/j.est.2022.106336.
[38] W.-l. Cheng, R.-m. Zhang, K. Xie, N. Liu, J. Wang, Heat conduction enhanced shape-stabilized paraffin/HDPE composite PCMs by graphite addition: preparation and thermal properties, Sol. Energy Mater. Sol. Cell. 94 (2010) 1636–1642, https://doi.org/10.1016/j.solmat.2010.05.020.
[39] C. Xiao, G. Zhang, Z. Li, X. Yang, Custom design of solid–solid phase change material with ultra-high thermal stability for battery thermal management, J. Mater. Chem. A 8 (2020) 14624–14633, https://doi.org/10.1039/D0TA05247G.
[40] V.G. Choudhari, D.A.S. Dhoble, T.M. Sathe, A review on effect of heat generation and various thermal management systems for lithium ion battery used for electric vehicle, J. Energy Storage 32 (2020), 101729, https://doi.org/10.1016/j.est.2020.101729.
[41] W. Situ, G. Zhang, X. Li, X. Yang, C. Wei, M. Rao, et al., A thermal management system for rectangular LiFePO4 battery module using novel double copper mesh-enhanced phase change material plates, Energy 141 (2017) 613–623, https://doi.org/10.1016/j.energy.2017.09.083.
[42] RT35HC data sheet, Rubitherm. https://www.rubitherm.eu/media/products/datasheets/Techdata_-RT35HC_EN_09102020.PDF. (Accessed 28 July 2023).
[43] A. Sarı, Form-stable paraffin/high density polyethylene composites as solid–liquid phase change material for thermal energy storage: preparation and thermal properties, Energy Convers. Manag. 45 (2004) 2033–2042, https://doi.org/10.1016/j.enconman.2003.10.022.

[44] Z.W. Ma, P. Zhang, Modeling the heat transfer characteristics of flow melting of phase change material slurries in the circular tubes, Int. J. Heat Mass Tran. 64 (2013) 874–881, https://doi.org/10.1016/j.ijheatmasstransfer.2013.05.026.
[45] T.L. Bergman, T.L. Bergman, F.P. Incropera, D.P. DeWitt, A.S. Lavine, Fundamentals of Heat and Mass Transfer, eighth ed., Wiley, 2018.
[46] M. Bahrami, Forced convection heat transfer. https://www.sfu.ca/~mbahrami/ENSC%20388/Notes/Forced%20Convection.pdf. (Accessed 28 July 2023).